DNA Toroids: Stages in Condensation†

Roxana Golan, Lía I. Pietrasanta, Wan Hsieh, and Helen G. Hansma*

Department of Physics, University of California, Santa Barbara, California 93106

Received April 19, 1999; Revised Manuscript Received August 2, 1999

ABSTRACT: The effects of polylysine (PLL) and PLL−asialoorosomucoid (AsOR) on DNA condensation have been analyzed by AFM. Different types of condensed DNA structures were observed, which show a sequence of conformational changes as circular plasmid DNA molecules condense progressively. The structures range from circular molecules with the length of the plasmid DNA to small toroids and short rods with ∼1/6 to 1/8 the contour length of the uncondensed circular DNA. Single plasmid molecules of 6800 base pairs (bp) condense into single toroids of ∼110 nm diameter, measured center-to-center. The results are consistent with a model for DNA condensation in which circular DNA molecules fold several times into progressively shorter rods. Structures intermediate between toroids and rods suggest that at least some toroids may form by the opening up of rods as proposed by Dunlap et al. [(1997) *Nucleic Acids Res. 25*, 3095]. Toroids and rods formed at lysine:nucleotide ratios of 5:1 and 6:1. This high lysine:nucleotide ratio is discussed in relation to entropic considerations and the overcharging of macroions. PLL−AsOR is much more effective than PLL alone for condensing DNA, because several PLL molecules are attached to a single AsOR molecule, resulting in an increased cation density.

DNA condensation has been studied for over 25 years (*1, 2*). In the early years the main question regarding DNA condensation was the following: How does DNA condense into the heads of bacteriophages? Now there is a new interest in DNA condensation, because DNA condensation is an important step in gene delivery for gene therapy (*3*).

Conventional techniques for investigating DNA condensation include circular dichroism and absorption spectroscopy (*4*), transmission electron microscopy (TEM), and light scattering (*5*−*7*). Atomic force microscopy (AFM)[1] is a valuable addition to these techniques, because the AFM visualizes DNA condensates in three dimensions with subnanometer height resolution (*8*). The AFM also images samples either dried or under near-physiological conditions (*9*−*11*). DNA condensation is easily analyzed by AFM, as many groups have shown (*12*−*19*).

DNA molecules condense into toroids and short rods under many different conditions. Most of the conditions for forming toroids involve some sort of polycation: trivalent cations (*20*), spermidine (*16*), protamine (*14*), polylysine (*2, 19*), and even positively charged surfaces (*15*).

Traditionally it has been believed that toroids are of a constant size with an outer diameter of 50 nm and an inner diameter of 15 nm. Toroids of approximately this size have been observed with DNA lengths from 400 to 56 000 base pairs (bp) (*21*). More recent results are showing that the variability of toroid sizes is actually considerably larger, as described below.

When toroids and rods are formed under the same conditions, they usually have similar contour lengths and similar widths (toroid widths = $R_{out} - R_{in}$). For example, both the toroids and the rods formed after a 2 h incubation in cobalt hexaammine have contour lengths of ∼200 nm and widths of ∼30 nm (*20*).

Toroids and rods form in different sizes when different conditions are used for preparing them. For most conditions, the sizes of toroids and rods vary over a 2-fold range: 100−200 nm contour lengths and 20−40 nm widths (*2, 14, 15, 20*). These contour lengths for toroids correspond to center-to-center diameters of 30−70 nm. There are exceptions to this, however: toroids with contour lengths of 300−400 nm (*15*) and huge toroids or ellipsoids with contour lengths on the order of 2 μm (*16*). In these two investigations, the toroid size depended on the concentration (*16*) or the length (*15*) of the DNA.

The DNA content of toroids and rods is often estimated by assuming that the toroid or rod has a crystalline B-DNA packing throughout (*20, 22*). Such calculations give a DNA content for a typical toroid or rod of ∼25 000−50 000 base pairs (bp).

The relationship between toroids and rods is another unknown in DNA condensation. Some investigators assume that DNA is coiled in toroids (*22*) which raises questions about how rods are formed. Other possibilities are that a DNA rod bends around (*23*) or opens up (*13*) to form a toroid.

These questions are addressed here for DNA condensed with PLL and PLL−asialoorosomucoid (AsOR). DNA condensations with PLL and PLL−AsOR have been imaged by TEM and AFM (*2, 19, 24, 25*). AsOR is a glycoprotein that binds to the liver cell receptor for asialoglycoproteins. AsOR−DNA condensates are designed for delivering genes on the DNA into liver cells (*26*).

† This work was supported by NSF Grant MCB 9604566 (H.G.H., W.H., L.I.P.) and NSF Grant DMR 9632716 (R.G.).

* Correspondence should be addressed to this author at the Department of Physics, UCSB, Santa Barbara, CA 93106. Telephone: (805) 893 3881. Fax: (805) 893 8315. Email: hhansma@physics.ucsb.edu.

[1] Abbreviations: AFM, atomic force microscope/microscopy; PLL, poly-L-lysine; AsOR, asialoorosomucoid; bp, base pair(s); kD, kilodalton(s); Da, dalton(s); fwhm, full width at half-maximum height.

10.1021/bi990901o CCC: $18.00
Published on Web 10/01/1999

MATERIALS AND METHODS

Substrates. Disks of mica (Ruby Muscovite Mica; New York Mica Co., New York, NY) were glued to steel disks with 2 ton epoxy resin (Devcon Corp.; Wood Dale, IL) and cleaved with adhesive tape immediately before use.

Samples. Complexes of DNA + PLL−AsOR were prepared in neutral saline (0.15 M NaCl) and in alkaline saline (0.15 M NaCl, 2 mM NaOH) as specified below. The DNA concentration was 10 ng/μL for all complexes. The DNA plasmid was pCMV luciferase (6832 bp) except as noted.

Poly-L-lysine (PLL) of two different sizes was used: 4 kDa (4kD PLL) and 10 kDa (10kD PLL). PLL−AsOR conjugates were prepared by carbodiimide coupling (*27*, *28*) at a 1:1:0.5 (w/w) ratio of AsOR to PLL to carbodiimide (EDC, 1-ethyl-3-[3-(dimethylamino)propyl]carbodiimide). EDC forms covalent amide bonds between AsOR carboxyl groups and PLL ϵ-amino groups.

The PLL−AsOR conjugates were purified on a Fast Flow Q Sepharose anion exchange chromatography column (Pharmacia) eluted with 50 mM Tris, pH 7.5. Conjugates were further purified by exhaustive dialysis against ultrapure water to remove PLL that did not react with AsOR (*27*).

The ratio of AsOR to PLL in these conjugates was 1:1 (w/w), as determined by the following method: An aliquot was lyophilized, weighed, and dissolved in ultrapure water at a specific concentration (w/v). Since PLL has minimal absorbance at 280 nm ($A_{280} = 0.0015$ mL mg^{-1} cm^{-1}), the AsOR component was calculated from the absorbance at 280 nm, using an extinction coefficient of 0.92 mL mg^{-1} cm^{-1}. The composition of the conjugate was determined by comparison of the concentration of the conjugate (w/v) with the concentration of AsOR (w/v) as measured by the absorbance at 280 nm. The difference between the two measurements was attributed to the PLL component of the conjugate (*27*).

Since the ratio of AsOR to PLL was 1:1 both before and after reaction with EDC, it would appear that the reaction proceeded to completion. This is a reasonable result, given the high concentration of EDC in the reaction mixture. Furthermore, there is a considerable excess of sites on AsOR to which PLL can attach. AsOR molecules have 31 acidic amino acid residues capable of reacting with PLL. At a 1:1 (w/w) ratio of AsOR to PLL, there is an average of only 4 PLL molecules of 10 kDa per AsOR molecule or 10 PLL molecules of 4 kDa per AsOR molecule.

The ratio of conjugate to DNA (w/w) necessary for specific ratios of lysine to nucleotide (lys:nt) was then calculated using the conjugate composition as determined by the above method (*27*). The molecular mass of AsOR is 38 kDa. The molecular mass of each lysine residue in PLL is 209 Da. PLL is sold as the HBr salt, with all lysine residues in the HBr form (Sigma, personal communication). Therefore, 209 Da = 146 Da (lysine) + 81 Da (HBr) − 18 Da (H_2O removed during polymerization).

These solutions and DNA complexes were prepared at the Immune Response Corp. (Carlsbad, CA) (*27*) and provided for AFM imaging at UCSB.

Sample Preparation. The AFM samples were prepared by placing 1−5 μL of solution on a freshly cleaved mica surface. After 60 s, they were rinsed with 1−2 mL of water, dried with a stream of compressed air, and further dried in a desiccator over P_2O_5.

AFM Imaging. Tapping-mode AFM was performed in dry nitrogen using a Nanoscope III AFM (Digital Instruments, Santa Barbara, CA). Bungee cords were used for vibration isolation (*29*). The D scanner was used for all samples. The scanner was accurate to 8% in the *x* and *y* directions, and was calibrated using a known grating. Standard silicon cantilevers 125 μm in length were used. Cantilever oscillation frequency was tuned to the resonance frequency of the cantilever, 280−350 kHz. The 256 × 256 pixel images were captured with a scan size between 0.24 and 4 μm at a scan rate of 2−6 scan lines per second.

Image Analysis. Images were processed by flattening using Nanoscope software in order to remove background slope. Height and full-width at half-maximum height (fwhm) were measured using the Nanoscope software. In the analysis of widths, the fwhm measurements were used as a first-order compensation for the systematic distortions introduced by the conical tip geometry (*30*). The contour lengths of DNA molecules and condensed DNA complexes were measured using NIH−Image software v.1.59 (National Institutes of Health, Bethesda, MD). The apparent volumes of the complexes were measured using the bearing analysis function of the Nanoscope software.

Statistics. Data are given as mean ± standard error of the mean (SEM). Significant differences in the results were evaluated by applying both Student's *t*-test and the Wilcoxon test when applicable ($P < 0.05$ or less). We analyzed 65 toroids and 29 rods.

RESULTS

DNA and PLL−AsOR condensed into a variety of complexes, depending on the ratio of lysine to nucleotides (lys:nt) (Figure 1). Clean backgrounds observed in AFM images lead to the conclusion that the solution ratios of lys:nt are close to the ratios of lys:nt in the DNA complexes. Uncomplexed DNA and PLL−AsOR were not observed in these images.

Typical circular plasmid DNA molecules are shown in Figure 1a. Complexes of the following morphologies were observed upon the addition of 4kD PLL−AsOR or 10kD PLL−AsOR: The flattened morphology of Figure 1b occurred with the addition of 4kD PLL−AsOR to DNA at a lys:nt ratio of 3:1 or 5:1. Note the thickening and shortening of the DNA strands. A further increase of the lys:nt ratio to 6:1 resulted in a further condensation of the DNA + 4kD PLL−AsOR complex, forming compact, oval-shaped molecules (Figure 1c). Replacing the 4kD PLL with 10kD PLL at a lys:nt ratio of 5:1 or 6:1 resulted in further condensation of the molecules into short rods and toroids (Figure 1d).

Line plots of eight DNA toroids show that these toroids are often regular in size and shape (Figure 2a−d) but are also seen in a variety of irregular sizes and shapes (Figure 2e−h). In addition, many structures are intermediate between rods and toroids (Figure 3b−f).

Measurements of Complexes. The measured height of the toroids was 3.7 ± 0.1 nm (mean ± SEM, $N = 65$) compared to the 0.3 ± 0.1 nm height of the plasmid shown in Figure 1a. The outer diameter was 142.1 ± 3.1 nm; the full width

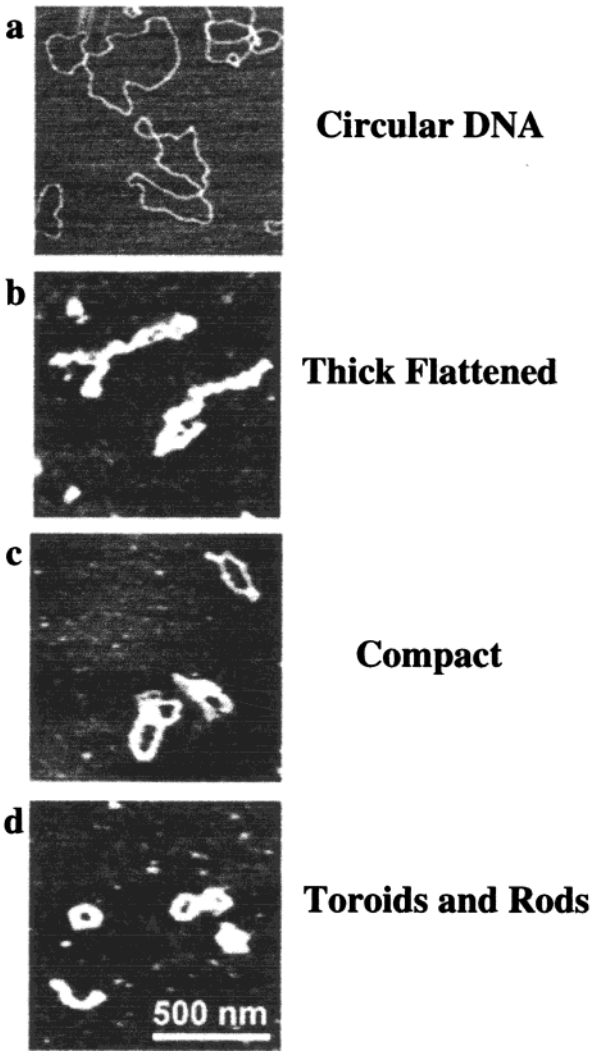

FIGURE 1: Stages in DNA condensation. AFM images of (a) circular plasmid DNA, 6800 bp. (b) Thick flattened complexes were observed in samples containing DNA + 4kD PLL−AsOR at a lys:nt ratio of 5:1. (c) Compact complexes were observed in samples containing DNA + 4kD PLL−AsOR at a lys:nt ratio of 6:1. Compact complexes also formed with DNA + 10kD PLL−AsOR with a lys:nt ratio of 1.6:1 (not shown). (d) Toroids and rods were observed in samples containing DNA + 10kD PLL−AsOR at a lys:nt ratio of 6:1. Rods and toroids were also seen with lys:nt = 5:1 (not shown). Images are 1.1 × 1.1 μm.

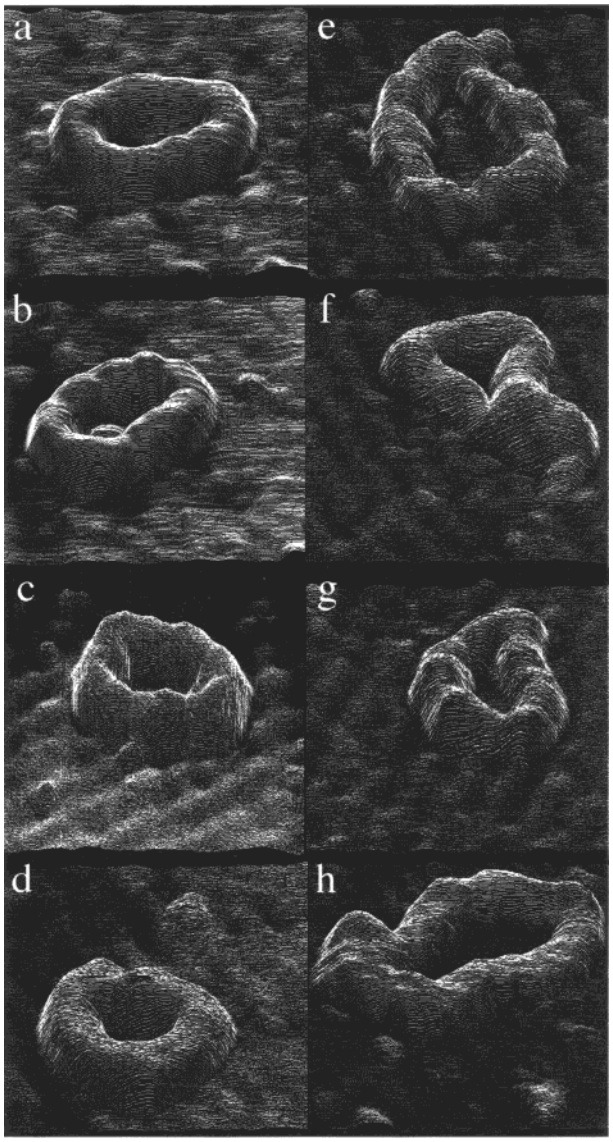

FIGURE 2: Variability in toroid size and shape. (a−d) Toroids of uniform shape and contour length. (e−h) Toroids of irregular shape and variable contour length. Line plots at 60° viewing angle emphasize topography. Composition of samples is the same as in Figure 1d. Maximum heights of features on toroids are ∼5−6 nm. Images are 250 × 250 nm.

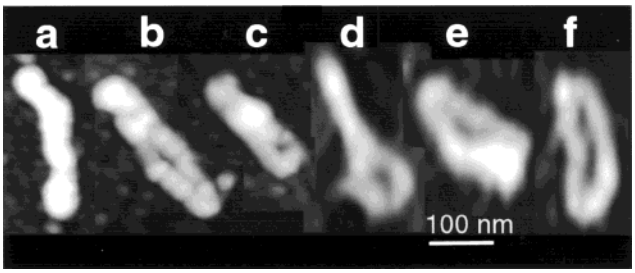

FIGURE 3: Intermediate structures between rods and toroids. A typical rod (a) and several condensed structures that are neither rods nor toroids (b−f) are seen under the condensation conditions of Figure 1d. These structures provide clues to the way in which DNA might condense in toroids and rods.

at half-maximum height (fwhm) of the toroid cross section was 44.1 ± 0.5 nm. Similarly, for the rods, the height was 3.9 ± 0.2 nm, and the width (fwhm) was 50.7 ± 1.7 nm. The measured widths of DNA, toroids, and other complexes are broadened by an amount comparable to the width and shape of the micro-tip used to image them (*30, 31*).

The average contour length for toroids and rods was significantly different: 339 ± 12 nm for toroids and 267 ± 8 nm for rods. The measured contour length of the plasmid DNA was 2280 ± 27 nm. This corresponded to a helical rise of 0.33 ± 0.01 nm/bp, which is in good agreement with the expected value of 0.34 nm/bp for B-DNA (*32*). The contour length for toroids gives an average center-to-center diameter of 108 nm for the toroids.

Volumes of Complexes. We have measured the volumes of thick flattened complexes, rods, and toroids (Figure 4). The results support the hypothesis that a single plasmid molecule condenses into a single complex: a thick flat complex or a toroid or a rod. For thick flattened complexes, the mean volume of the majority of the complexes is ∼50 000 nm^3. The two very large complexes in Figure 4a look like double complexes and have volumes that are about twice as large.

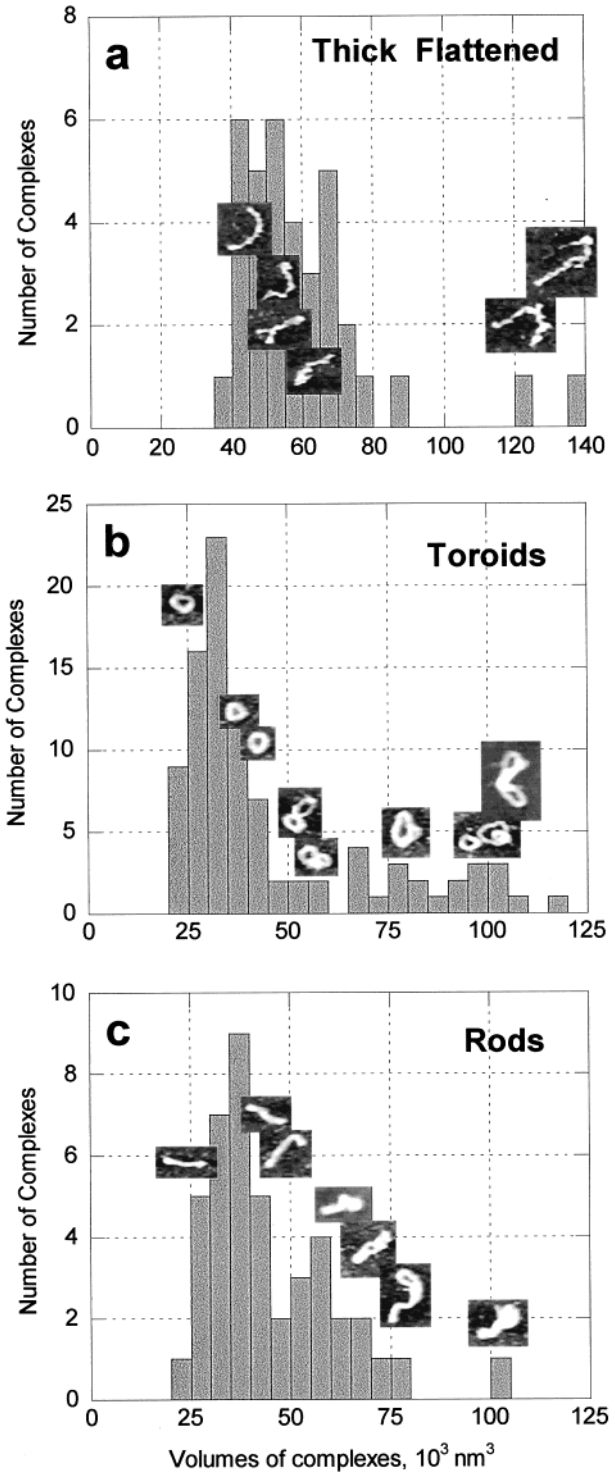

FIGURE 4: Volumes of condensed DNA complexes. Histograms show the volume distributions for (a) thick flattened complexes, (b) toroids, and (c) rods. Volumes of toroids and rods are not significantly different. The initial peak of each histogram corresponds to complexes containing a single plasmid DNA molecule. The AFM images of thick flattened complexes are at a smaller scale than those of toroids and rods; their relative sizes are shown in Figure 1b,d and Figure 5. The compositions of rods, toroids, and thick flattened complexes are the same as in Figure 1b,d.

Similarly, for the toroids and rods in Figure 4b,c, the majority of the complexes cluster in a peak with mean volumes of 32 500 nm^3 for toroids and 34 700 nm^3 for rods. There were no complexes with volumes below ~20 000 nm^3, and the complexes with larger volumes were clustered at volumes that were 2 or 3 times as large: ~60 000 nm^3 for rods; ~70 000 nm^3 and ~100 000 nm^3 for toroids. Again, these results are consistent with the hypothesis that most condensed DNA complexes contain single DNA molecules, while a few complexes contain two or three DNA molecules.

Note (i) the similar volumes obtained for the rods and toroids, indicating a similar degree of condensation in both structures despite the different morphologies, and (ii) the smaller volumes in the rods and toroids compared to the thick flattened complexes, suggesting that the higher degree of condensation in rods and toroids results in the contribution of less tip volume than in thick flattened complexes, which have a longer contour length in contact with the AFM tip. The apparent width of structures in AFM images is broadened by an amount comparable to the width of the tip that interacts with the structures.

The contribution of the AFM tip to volume measurements can be minimized for structures of uniform height by measuring the volume of the top half of the structure. The total volume of the structure is defined to be twice the volume measured for the top half of the structure (*33*). For toroids and rods, the apparent volumes were also calculated (data not shown) from the height and the fwhm by a variation of the method of ref *33*. The calculated and the measured apparent volumes were in good agreement. This is further evidence for the reliability of the volumes shown in Figure 4.

Quantifying Condensation. We have measured the condensation of DNA complexes that, from their volumes, appeared to have single DNA molecules. A gallery of these DNA complexes at different condensations is shown in Figure 5, which correlates the morphology of the complexes with the degree of condensation during the process of folding. The images in Figure 5 show DNA complexes at all stages of condensation, from samples prepared in the various ways described in Figure 1.

Figure 5 illustrates the definition of DNA condensation: the extent of DNA condensation is defined as the ratio between the contour length of the plasmid and the contour length of the condensed complex.

For thick flattened complexes, the average condensation is 2.6 (Figure 6a). For compact complexes, the average condensation is 3.9, with a range of ~3−5.5 (Figure 6b). For toroids and rods, the average condensation ratios are 6.7 and 8.5, respectively (Figure 6c,d). Note that the variability in condensation is clearly smaller in rods than toroids.

DISCUSSION

In this work, we have used the AFM to analyze the extent of DNA condensation in complexes of DNA with PLL covalently attached to the glycoprotein asialoorosomucoid (AsOR), as described in Figure 1. The degree of DNA condensation increased progressively as the amount of PLL−AsOR increased in the complexes. The degree of DNA condensation also increased with a longer PLL chain, resulting in compact toroids and short rods. In contrast, DNA condensation was weak with PLL alone as observed by AFM (Figure 7) (*19*).

PLL−AsOR vs PLL Alone. This posed a puzzle: why the negatively charged glycoprotein, AsOR, covalently attached to PLL, could enhance the condensation of DNA so much

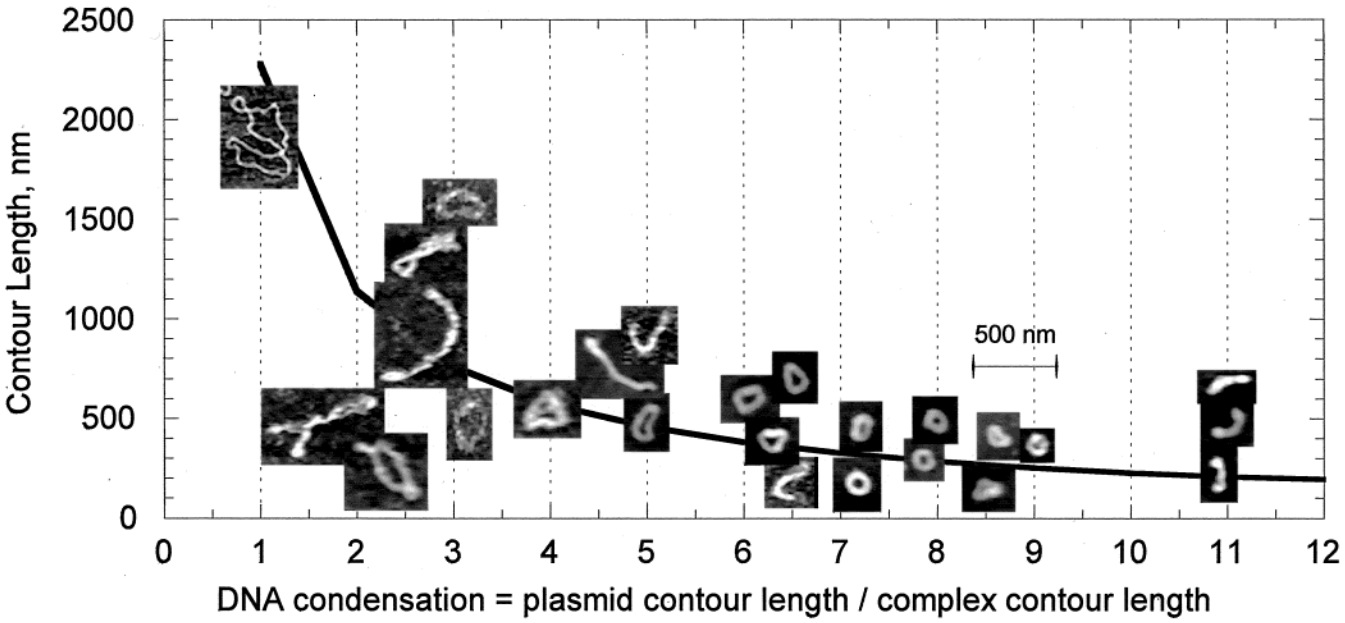

FIGURE 5: An illustrated graph of DNA condensation. DNA condensation is defined as: (contour length of the plasmid)/(contour length of the condensed complex). AFM images are placed on the graph at the *x*-coordinate of their DNA condensation; the correct *y*-coordinate for each AFM image is indicated by the graph line. AFM images are from samples of all the compositions described in Figure 1. Scale bar = 500 nm for all images.

over the condensation caused by the polycation, PLL, alone. We suggest that AsOR condenses DNA by bringing together several molecules of PLL onto a single AsOR molecule, thus increasing the cation density and facilitating the condensation of DNA into compact toroids and rods (Figure 8). PLL is a much weaker condensing agent than PLL−AsOR, as evaluated by this AFM assay.

10kD PLL−AsOR vs 4kD PLL−AsOR. 10kD PLL−AsOR condenses DNA into toroids and rods, as illustrated in Figure 8, while 4kD PLL−AsOR does not. This result was not expected a priori, since 10kD PLL−AsOR and 4kD PLL−AsOR have the same number of positively charged lysine residues per PLL−AsOR conjugate.

The scale model in Figure 8 gives an insight into why larger PLL molecules condense DNA better than smaller PLL molecules when attached to AsOR. It shows that 10kD PLL molecules project further from AsOR than 4kD PLL molecules. Therefore, AsOR with 10kD PLL has a larger number of accessible positive charges on the PLL molecules, as compared with 4kD PLL−AsOR.

Folding and Coiling. There are at least three possible ways in which DNA might condense in the presence of PLL−AsOR. First, DNA might coil into chromatin-like structures, in which DNA wraps around PLL−AsOR to form nucleosome-like structures that then coil into a fiber. Second, DNA might coil around the circumference of a toroid, like thread on a spool. Third, DNA might fold into successively shorter structures.

The rods and toroids are similar in thickness to 30 nm chromatin fibers. They also have lumps that are consistent with a modular structure, as in chromatin fibers. The lumps are visible in, e.g., Figures 2e,g and 3a,b. Chromatin fibers are formed from nucleosomes in which ~200 bp (~70 nm) DNA wraps around a histone octamer of 110 kDa to form an 11 nm structure (*34*). This results in DNA condensation of 6 or more, which is considerably higher than the condensation observed here for early stages of DNA condensation with PLL−AsOR (Figures 1, 5, 6). The results with 10kD PLL−AsOR vs 4kD PLL−AsOR are also consistent with a folding/coiling model for the structure of these toroids, as opposed to a chromatin-like model. The PLL−AsOR complex that condenses DNA much more effectively is 10kD PLL−AsOR, with ~4 long PLL chains, not 4kD PLL−AsOR, which is more compact like the histone core of the nucleosome. X-ray scattering results with other DNA toroids also indicate that the DNA in these toroids is arranged in parallel rows (*35*, *36*), which is again consistent with condensation by folding or coiling and not with a chromatin-like condensation for other DNA toroids and rods.

Although we cannot rule out some nucleosome-like condensation, we do see clear evidence for folding in many of the condensed DNA complexes. For example, the thick flattened complexes and compact complexes of Figure 1b,c show visual evidence of DNA folding as a mechanism for DNA condensation. Folding is the most likely means of condensing a circular plasmid into a linear complex with a 2-fold condensation. But this linear complex could further condense by folding and/or coiling.

Both folding and coiling may occur. If the ends of the linear complex overlap in an antiparallel direction, the complex will form a hairpin-like fold. If the ends of the linear complex overlap in a parallel direction, they will form the beginning of a coil, which will grow as the ends of the complex continue to wrap around the circumference of the incipient coil.

Successive folding in half would predict peaks in DNA condensation at 2, 4, 8. Rods fit the folding model because they have a mean condensation of 8 (Figure 6d). Toroids have a much broader condensation distribution (Figure 6c) and may condense by both coiling and folding. Some toroids may form from rods that open into toroids, as in the rod-to-toroid intermediates of Figure 3b−f. Such a mechanism has been proposed by Dunlap et al. (*13*), based on their beautiful AFM images of condensed DNA in fluid.

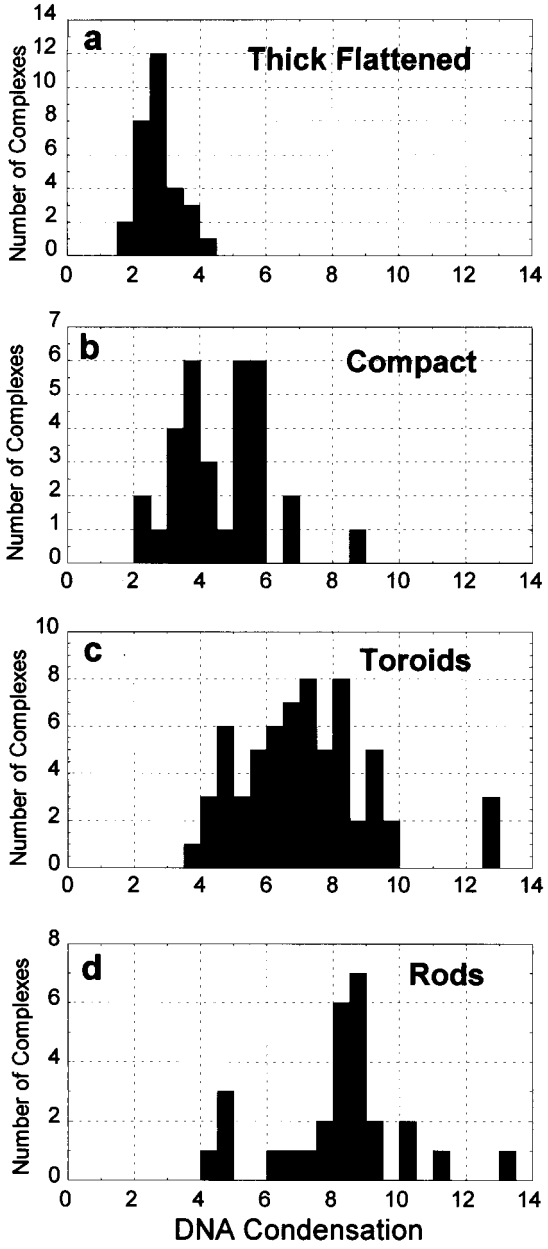

FIGURE 6: Extent of DNA condensation. Histograms show the DNA condensation distribution for (a) thick flattened complexes, (b) compact complexes, (c) toroids, and (d) rods. The composition of each type of DNA complex is described in Figure 1. DNA condensation is defined in Figure 5.

DNA condensation with PLL−AsOR is probably dominated by electrostatic interactions. Such interactions are the most common cause of DNA condensation (*37*). For example, DNA condensation becomes spontaneous in the presence of tri- or tetravalent cations in aqueous solutions as a result of the large decrease in the electrostatic repulsion between charged DNA segments (*21*, *38*). Supercoiling of the plasmid DNA may also contribute to the form of these DNA condensates with PLL−AsOR, but supercoiling is not required for DNA toroid formation (*20*).

Toroid Calculations. The measured volumes for these toroids and rods are close to the calculated volume for a toroid or rod containing 1 plasmid DNA molecule and 5−6 lys:nt. The calculations are as follows:

The mean volumes of single toroids are ∼30 000−35 000 nm^3, as measured from AFM images (Figure 4). Volumes

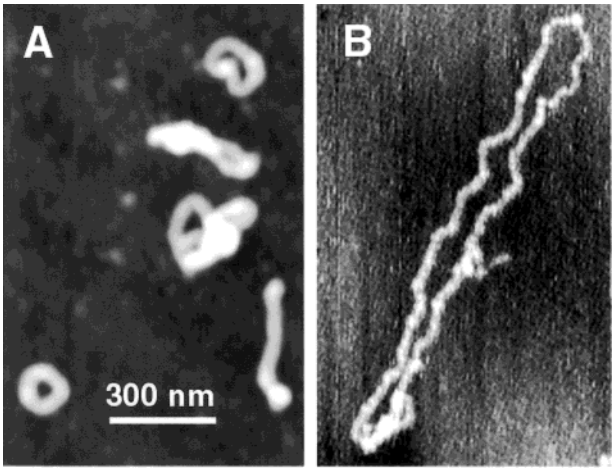

FIGURE 7: Comparison of PLL and PLL−AsOR for condensing DNA. AsOR enhances the condensation of individual DNA molecules. (a) DNA + 10kD PLL−AsOR, lys:nt = 5:1. (b) DNA + 26kD PLL, lys:nt = 3:1. DNA condensed with higher lys:nt did not show further condensation.

measured from AFM images are typically comparable to the volumes calculated from molecular weights, using a density of 1−1.3 g/mL (*33*, *39*).

The plasmid volume is 7000 nm^3, based on the dimensions of B-DNA from X-ray crystallography. The molecular volume of 10kD PLL−AsOR is ∼100 nm^3, calculated from its molecular mass of ∼80 kDa and a density of 1−1.3 g/mL. Each molecule of 10kD PLL−AsOR has ∼320 lysine residues (Figure 8 caption). Therefore, for 5−6 lys:nt and 14 000 nt per plasmid DNA molecule, there are ∼200−300 10kD PLL−AsOR molecules per plasmid DNA molecule, or ∼25 000 nm^3 PLL−AsOR. The sum of the calculated volumes for DNA and PL−AsOR is ∼32 000 nm^3, which is within the range of volumes measured for toroids from AFM images.

High lys:nt Ratio. It has been suggested that the high lys:nt ratio in these toroids and rods may be related to 'overcharging', or excess negative charge seen in theoretical condensates of large flexible polyanions with large rigid polycations. The overcharging in these theoretical condensates has been attributed to an entropic release of counterions from the flexible polyanion (*40*) and may be related to the overcharging of nucleosomes (*41*). Since DNA and PLL−AsOR are both flexible polyelectrolytes, the theories of overcharging are not directly related to these toroids and rods.

However, entropy does favor the high lys:nt ratio in these toroids and rods, because protons are released when DNA phosphates are anionic and PLL ϵ-amino groups are neutral. The presence of neutral lysine residues in PLL would raise the lys:nt ratio for toroids and rods above the 1:1 lys:nt ratio that would be predicted for a direct neutralization of DNA by PLL.

With 5−6 lysines per nucleotide, the average spacing between PLL−AsOR molecules along the DNA is 10 nm. Only ∼20% of the lysine residues are needed to neutralize charges on the DNA; the outer 20% of the lysine residues on each PLL chain are the most accessible and therefore perhaps the most likely to interact directly with the negatively charged phosphate groups on the DNA backbone.

The ends of these 30 nm long PLL arms can reach out to near strands of DNA, providing an electrostatic attraction

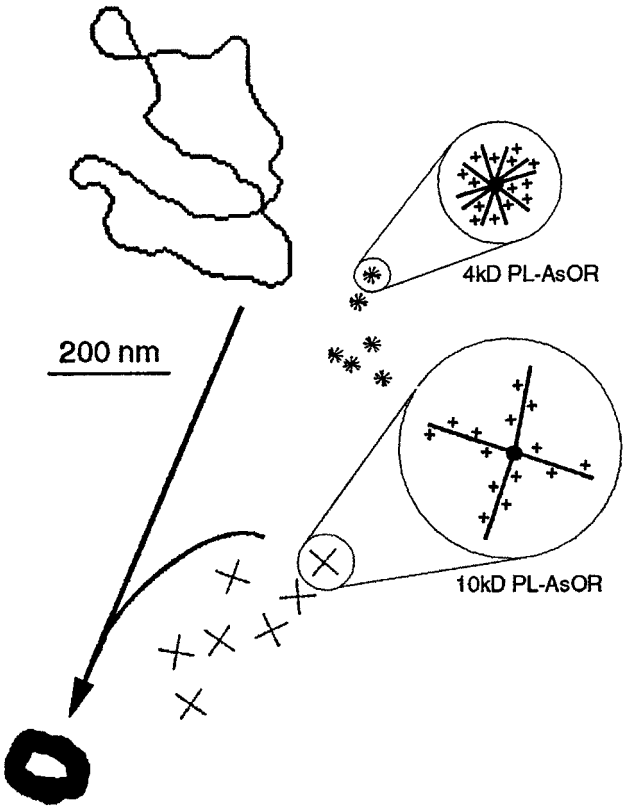

FIGURE 8: Scale model of DNA condensation. Scale diagrams of a plasmid DNA molecule, several molecules each of 10kD PLL−AsOR and 4kD PLL−AsOR, and a typical toroid. 10kD PLL has ∼80 lysine residues per molecule, giving a mean length of 27 nm; 4kD PLL has ∼30 lysine residues per molecule, giving a mean length of 11 nm. Magnified views of 10kD PLL−AsOR and 4kD PLL−AsOR show the charge and arrangement of polylysine chains on AsOR. AsOR is a 38 kDa glycoprotein with 30 acidic amino acid residues per molecule and a net charge of 5 carboxylic acid groups per molecule (*42*). The diameter of a globular protein of this size is ca. 5 nm. At a 1:1 (w/w) ratio of PLL to AsOR, there is an average of 4 molecules of 10kD PLL per AsOR molecule or 10 molecules of 4kD PLL per AsOR molecule. This corresponds to ∼300 lysine residues per AsOR molecule. Some PLL molecules probably attach to AsOR at multiple sites or at lysine residues closer to the center of the PLL molecule than in the diagram. Some PLL molecules probably attach to 2 AsOR molecules. These attachments are entropically and sterically less probable than the single end attachments shown in the diagram. Since toroids form with 10kD PLL−AsOR at a lys:nt ratio of 5:1 or 6:1, a single circular plasmid DNA molecule condenses with 300−400 10kD PLL−AsOR molecules into a toroid. 4kD PLL−AsOR is much less effective at condensing DNA and produces thick flat complexes and compact complexes with condensation ∼2−4 (see Figures 1, 6).

that pulls the DNA into compact structures. With a 6−8-fold DNA condensation in toroids and rods, the average AsOR spacing along the length of the toroid or rod is less than 2 nm. Each AsOR−PLL can reach with its 30 nm long PLL arms across the entire width of a toroid or rod. We hypothesize that the increase in entropy due to the release of bound water molecules in DNA and PLL−AsOR is larger than the decrease in entropy due to confinement of the DNA and the PLL−AsOR in the condensed structures.

In summary, we have observed stages in DNA condensation with PLL−AsOR that are consistent with a model for DNA condensation in which the DNA molecules coil into toroids or fold several times into progressively shorter rods, which can open up into toroids. Our results indicate that one plasmid molecule condenses into one condensed complex: thick flattened or compact or toroid or rod.

ACKNOWLEDGMENT

We thank Charlie Lollo and Deborah Kwoh of The Immune Response Corp. for providing the complexes of DNA with PLL−AsOR, Victor Bloomfield, Ioulia Rouzina, Sergei Leiken, William Gelbart, Stella Park, Avinoam Benshaul, Daniel Harrie, Fyl Pincus, and Moshe Kugler for helpful discussions, the reviewers for their insightful comments, and Scott Hansma for the software used to convert Nanoscope files into TIFF files.

REFERENCES

1. Evdokimov, Y. M., Platonov, A. L., Tikhonenko, A. S., and Varshavsky, Y. M. (1972) *FEBS Lett. 23*, 180−184.
2. Laemmli, U. K. (1975) *Biochemistry 14*, 4288−4292.
3. Phillips, S. C. (1995) *Biologicals 23*, 13−16.
4. Gosule, L. C., and Schellman, J. A. (1978) *J. Mol. Biol. 121*, 311−326.
5. Chattoraj, D. K., and Gosule, L. C. (1978) *J. Mol. Biol. 121*, 327−337.
6. Dodson, M., and Echols, H. (1991) *Methods Enzymol. 208*, 168.
7. Bloomfield, V. A. (1996) *Curr. Opin. Struct. Biol. 6*, 334−341.
8. Bustamante, C., and Rivetti, C. (1996) *Annu. Rev. Biophys. Biomol. Struct. 25*, 395−429.
9. Bustamante, C., Rivetti, C., and Keller, D. J. (1997) *Curr. Opin. Struct. Biol. 7*, 709−716.
10. Hansma, H. G., and Pietrasanta, L. (1998) *Curr. Opin. Chem. Biol. 2*, 579−584.
11. Czajkowsky, D. M., and Shao, Z. (1998) *FEBS Lett. 430*, 51−54.
12. Wolfert, M. A., and Seymour`, L. W. (1996) *Gene Ther. 3*, 269−273.
13. Dunlap, D. D., Maggi, A., Soria, M. R., and Monaco, L. (1997) *Nucleic Acids Res. 25*, 3095−3101.
14. Allen, M. J., Bradbury, E. M., and Balhorn, R. (1997) *Nucleic Acids Res. 25*, 2221−2226.
15. Fang, Y., and Hoh, J. H. (1998) *Nucleic Acids Res. 26*, 588−593.
16. Lin, Z., Wang, C., Feng, X., Liu, M., Li, J., and Bai, C. (1998) *Nucleic Acids Res. 26*, 3228−3234.
17. Kawaura, C., Noguchi, A., Furuno, T., and Nakanishi, M. (1998) *FEBS Lett. 421*, 69−72.
18. Hart, S. L., Arancibia-Cárcamo, C. V., Wolfert, M. A., Mailhos, C., O'Reilly, N. J., Ali, R. R., Coutelle, C., George, A. J., Harbottle, R. P., Knight, A. M., Larkin, D. F., Levinsky, R. J., Seymour, L. W., Thrasher, A. J., and Kinnon, C. (1998) *Hum. Gene Ther. 9*, 575−585.
19. Hansma, H. G., Golan, R., Hsieh, W., Lollo, C. P., Mullen-Ley, P., and Kwoh, D. (1998) *Nucleic Acids Res. 26*, 2481−2487.
20. Arscott, P. G., Li, A. Z., and Bloomfield, V. A. (1990) *Biopolymers 30*, 619−630.
21. Bloomfield, V. A. (1991) *Biopolymers 31*, 1471−1481.
22. Park, S. Y., Harries, D., and Gelbart, W. M. (1998) *Biophys. J. 75*, 714−720.
23. Marx, K. A. (1987) in *Structure and Dynamics of Biopolymers. NATO ASI Series. Series E, Applied Sciences; No. 133* (Nicolini, C. A., Ed.) pp 137−168, Nijhoff, Dordrecht and Boston.
24. Bunnell, B. A., Askari, F. K., and Wilson, J. M. (1992) *Somat. Cell Mol. Genet. 18*, 559−569.
25. Perales, J. C., Grossmann, G. A., Molas, M., Liu, G., Ferkol, T., Harpst, J., Oda, H., and Hanson, R. W. (1997) *J. Biol. Chem. 272*, 7398−7407.
26. Ruiz, J., and Wu, G. Y. (1998) *Biog. Amines 14*, 499−518.

27. Kwoh, D. Y., Coffin, C. C., Lollo, C. P., Jovenal, J., Banaszczyk, M. G., Mullen, P., Phillips, A., Amini, A., Fabrycki, J., Bartholomew, R. M., Brostoff, S. W., and Carlo, D. J. (1999) *Biochim. Biophys. Acta 1444*, 171−190.
28. McKee, T. D., DeRome, M. E., Wu, G. Y., and Findeis, M. A. (1994) *Bioconjugate Chem. 5*, 306−311.
29. Hansma, H. G., Bezanilla, M., Laney, D. L., Sinsheimer, R. L., and Hansma, P. K. (1995) *Biophys. J. 68*, 1672−1677.
30. Fritzsche, W., Schaper, A., and Jovin, T. M. (1994) *Chromosoma 103*, 231−236.
31. Bustamante, C., Vesenka, J., Tang, C. L., Rees, W., Guthold, M., and Keller, R. (1992) *Biochemistry 31*, 22−26.
32. Wing, R., Drew, H., Takano, T., Broka, C., Tanaka, S., Itakura, K., and Dickerson, R. E. (1980) *Nature 287*, 755−758.
33. Pietrasanta, L. I., Thrower, D., Hsieh, W., Rao, S., Stemmann, O., Lechner, J., Carbon, J., and Hansma, H. G. (1999) *Proc. Natl. Acad. Sci. U.S.A. 96*, 3757−3762.
34. Stryer, L. (1988) *Biochemistry*, 3rd ed., W. H. Freeman and Company, New York.
35. Maniatis, T., Venable, J. H., Jr., and Lerman, L. S. (1974) *J. Mol. Biol. 84*, 37−64.
36. Evdokimov, Y. M., Pyatigorskaya, T. L., Polyvtsev, O. F., Akimenko, N. M., Kadykov, V. A., Tsvankin, D. Y., and Varshavsky, Y. M. (1976) *Nucleic Acids Res. 3*, 2353−2366.
37. Rouzina, I., and Bloomfield, V. A. (1998) *Biophys. J. 74*, 3152−3164.
38. Marquet, R., Wyart, A., and Houssier, C. (1987) *Biochim. Biophys. Acta 909*, 165−172.
39. Schneider, S. W., Larmer, J., Henderson, R. M., and Oberleithner, H. (1998) *Pflugers Arch. 435*, 362−367.
40. Park, S. Y., Bruinsma, R. F., and Gelbart, W. M. (1999) *Europhys. Lett. 46*, 454−460.
41. Mateescu, E. M., Jeppesen, C., and Pincus, P. (1999) *Europhys. Lett. 46*, 493−498.
42. Baumann, P., Eap, C. B., Mueller, W. E., and Tillement, J.-P. (1989) *Alpha1-acid glycoprotein: genetics, biochemistry, physiological functions, and pharmacology;* proceedings of a meeting held in Prilly-Lausanne, Switzerland, September 1−2, 1988, Liss, New York.

BI990901O